

SFN 309 #31-40

藤井 通子

# 37. The High Mass Slope of the IMF

Antonio Parravano<sup>1,2\*</sup>, David Hollenbach<sup>3</sup> Christopher F. McKee<sup>4</sup>

- IMFのhigh-mass end ( $>1.5M_{\text{sun}}$ )の傾きは太陽近傍(1.7-2.1; Salpeterは1.35)と若い星団(1.2-1.7)で異なる。
- Massive star ( $>3M_{\text{sun}}$ )の寿命は短いのので、太陽近傍に均一に(uniformly)分布する前に死んでいるのでは？
- 星が死ぬことを考えて、太陽近傍で観測される現在の質量関数(present day mass function; PDMF)の傾き $\Gamma_{\text{app}}$ がどうなるかモデルを作ってみてみた。
- シミュレーション
  - $0 < x < 25 \text{ kpc}$  (銀河の動径方向),  $0 < y < 1.5 \text{ kpc}$  (接線方向)のシミュレーションボックス
  - 分子雲の分布を仮定、ランダムに生まれて20Myrの寿命
  - 分子雲からの星形成率を仮定して、べき $\Gamma$ に従って $1.5 < m < 6M_{\text{sun}}$ の星を生成
  - 星はガウス分布に従う速度分散を持つので、拡散する
  - 2.5Gyr星の運動を追って、いろんな場所を選んで $\Gamma$ の値を測った
  - ここで測るのは直接 $\Gamma$ ではなく、 $1.5 < m < 3M_{\text{sun}}$ と $3 < m < 6M_{\text{sun}}$ の星の割合でこれを使って $\Gamma$ を計算する

## 35. つづき

色の違いは最初に与える $\Gamma$ の違い

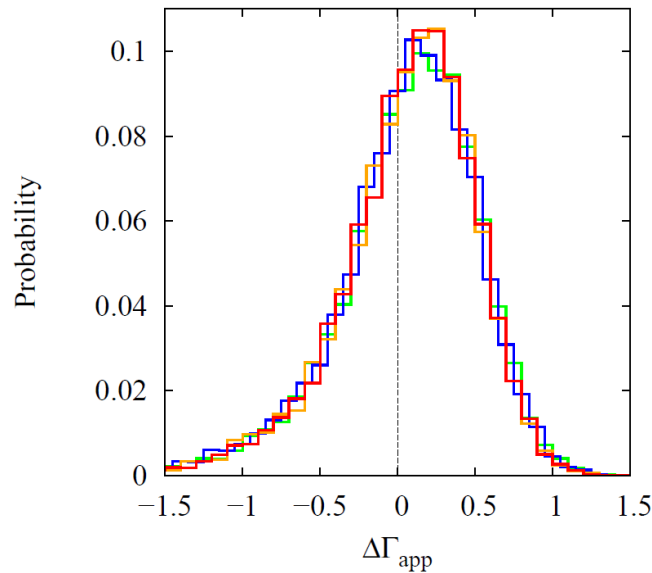
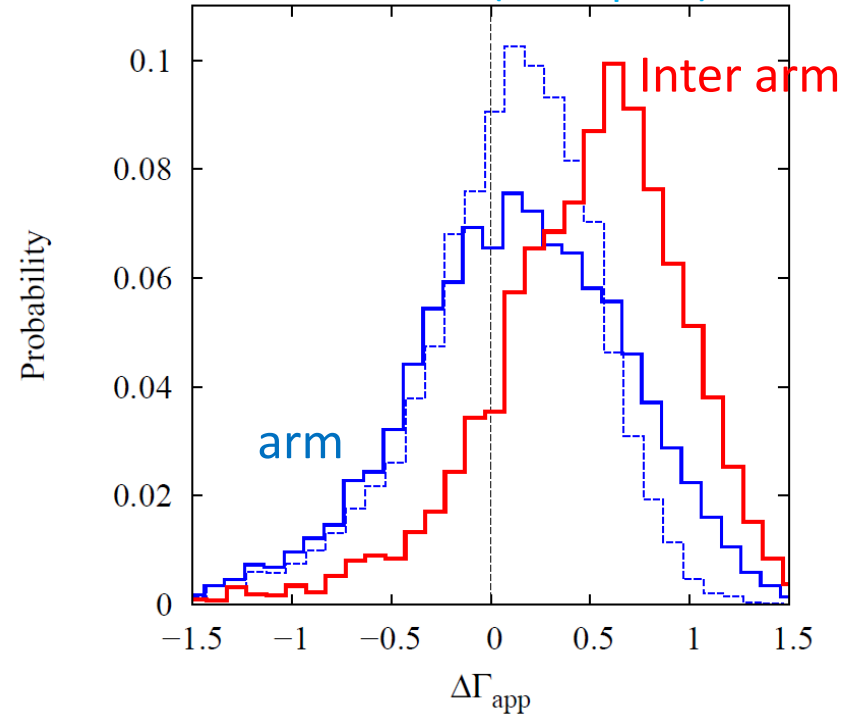


**Figure 2.** Probability distribution of  $\Delta\Gamma_{\text{app}}$  for four different values of the underlying  $\Gamma$ . Green is  $\Gamma = 1.2$ , blue is  $\Gamma = 1.35$ , orange is  $\Gamma = 1.5$ , and red is  $\Gamma = 1.7$ . The bin size is  $\Delta\Gamma_{\text{app}} = 0.05$ . The plots are essentially the same, showing that probability distribution of  $\Delta\Gamma_{\text{app}}$  does not depend on  $\Gamma$ . We assume here the standard stellar random velocity distribution and  $r_{\text{obs}} = 200$  pc.

Standard model (w/o spiral)



- $\Delta\Gamma(=\Gamma_{\text{app}} - \Gamma) > 0.35$  (観測を再現)する尤度(likelihood)は30%くらい
- 渦状腕があると考えて、渦状腕での分子雲形成率がinter-arm領域より高いと仮定する
- 太陽はinter-armにあるので、inter-arm領域のみで $\Gamma$ を測ると、 $\Delta\Gamma$ が0.35以上である尤度は50-60% (重い星はできた場所、つまりarm領域に集まっているから)

# 39. Outer solar system possibly shaped by a stellar fly-by

Susanne Pfalzner<sup>1</sup>, Asmita Bhandare<sup>1,2</sup>, Kirsten Vincke<sup>1</sup> and Pedro Lacerda<sup>3</sup>

Parameter	Simulated values
perturber mass	0.1, 0.3, 0.5, 1.0, 2.0 5.0, 10. 20, 50
periastron distance	30, 50, 100, 120, 150, 200, 250, 300, 500, 700, 1000
inclination	0,10,20,30,40,50,60,70,80,90,100,110,120,130,140,150,160,170,180
periastron angle	0, 45, 90

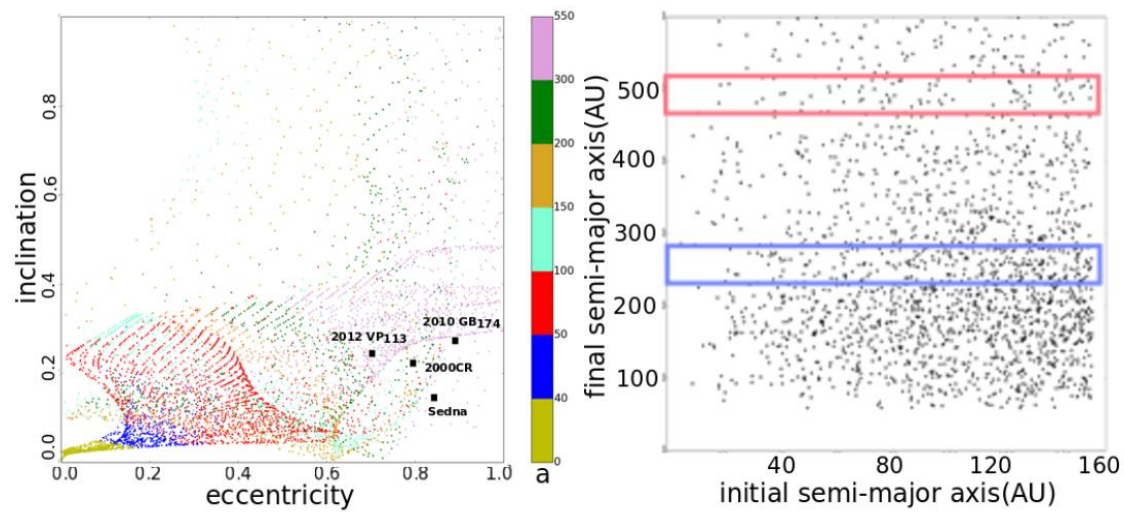
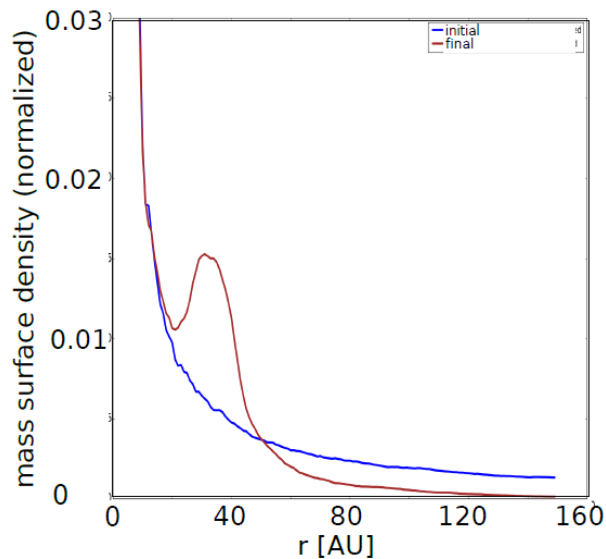
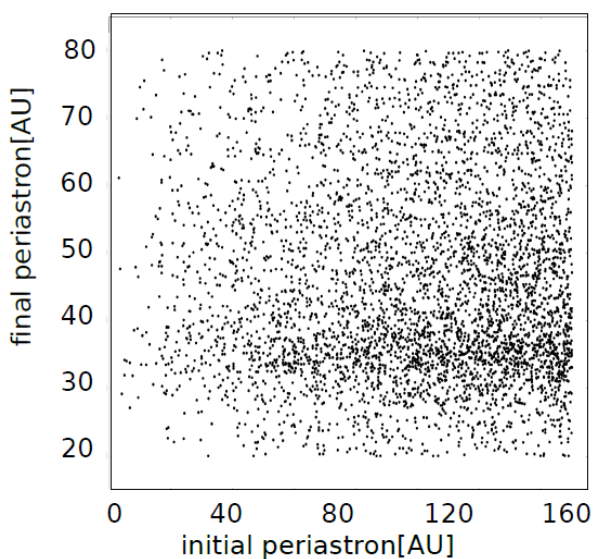


Figure 3. a) shows the eccentricity vs. inclination for all test particles for the fly-by illustrated in Fig. 2, with the properties of Sedna, 2012 VP<sub>113</sub>, 2000 CR and 2010 GB<sub>117</sub> indicated. b) shows the semi-major axis after the fly-by (final) of the test particles as a function of the pre-fly-by semi-major axis (initial). The areas relevant for Sedna (red) and 2012 VP<sub>113</sub> (blue) are high-lighted.

- 恒星遭遇によって、太陽系のTNO(海王星以遠天体)の離心率等が変わったのでは？
  - TNO全体の質量が予想されるより小さい
  - 離心率、軌道傾斜角が大きい
- 恒星遭遇があった時に惑星の軌道がどう変わるかN体計算した

# 39. つづき



- 面密度のbumpができる
- 天王星(14.6ME)より海王星(17.2EM)が重い理由かも

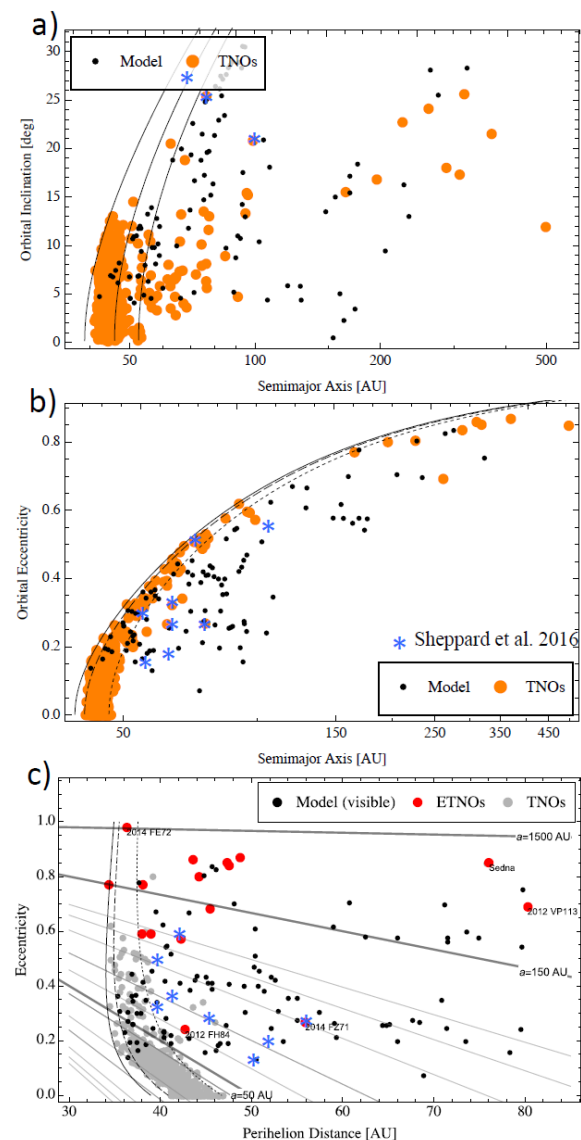
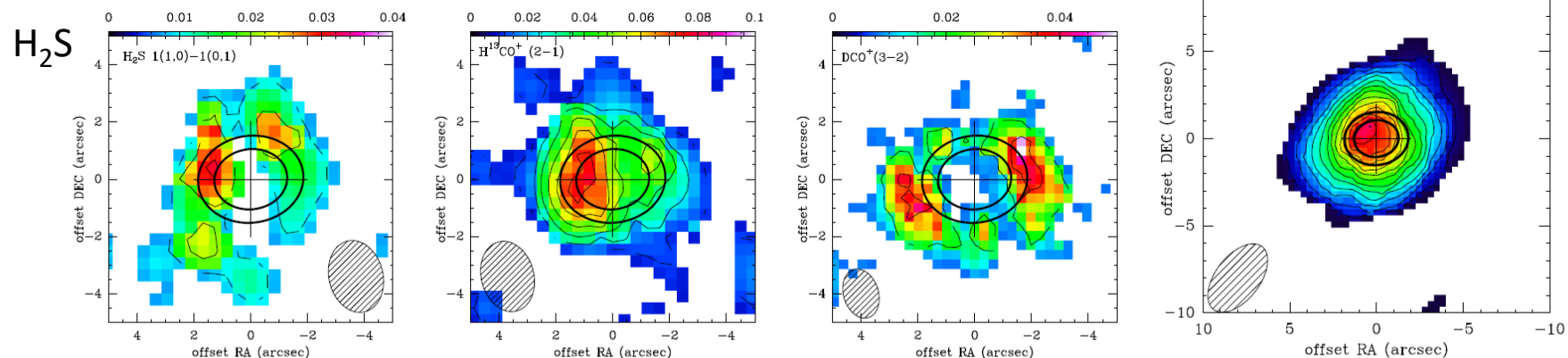


**Figure 4.** Resulting distribution of objects after the fly-by, where a) shows inclination vs. semi-major axis, b) eccentricity vs. semi-major axis and c) eccentricity vs. perihelion distance. The red symbols indicate the observed objects and the black symbols the predictions from the model.

# 40. First detection of $\text{H}_2\text{S}$ in a protoplanetary disk. The dense GG Tau A ring

N.T. Phuong<sup>1,2,3</sup>, E. Chapillon<sup>1,4</sup>, L. Majumdar<sup>5</sup>, A. Dutrey<sup>1</sup>, S. Guilloteau<sup>1</sup>, V. Piétu<sup>4</sup>, V.

## Integrated intensity map



リング: 180–260au

## Velocity map

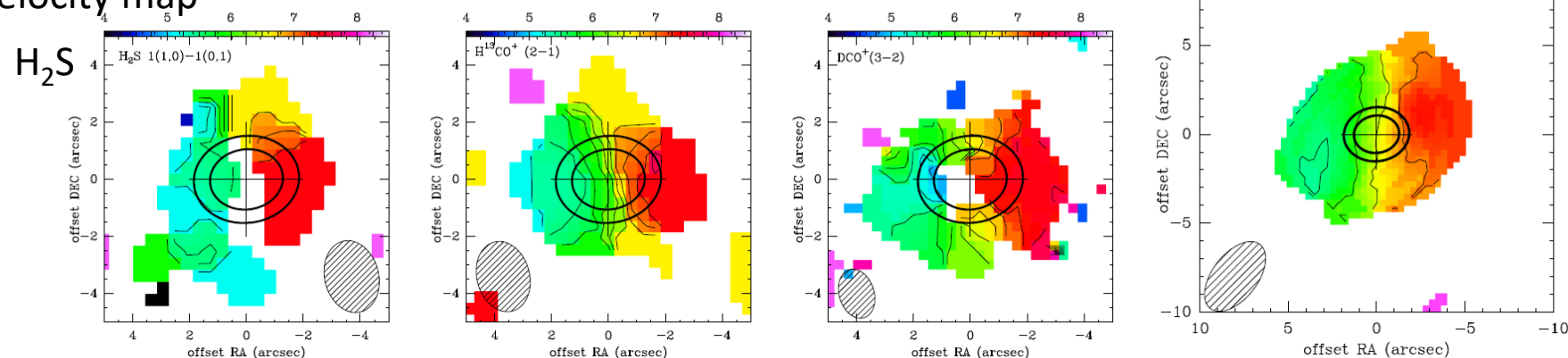


**Fig. 1.** Upper row: integrated intensity maps. The color scale is in the unit of  $(\text{Jy beam}^{-1} \text{ km s}^{-1})$ . Contour level step is  $2\sigma$ . Lower row: velocity maps. Contour level step is  $0.5 \text{ km s}^{-1}$ . Beam sizes are indicated. The ellipses show the location of inner ( $\sim 180 \text{ au}$ ) and outer ( $\sim 260 \text{ au}$ ) radii of the dust ring.

- GG Tau A の周りの冷たい高密度のリングから $\text{H}_2\text{S}$ のemissionを検出した。(NOEMA)

# 40. つづき

スケールハイトの3倍にピーク  
Grain surfaceでH2Sの80%が  
作られる

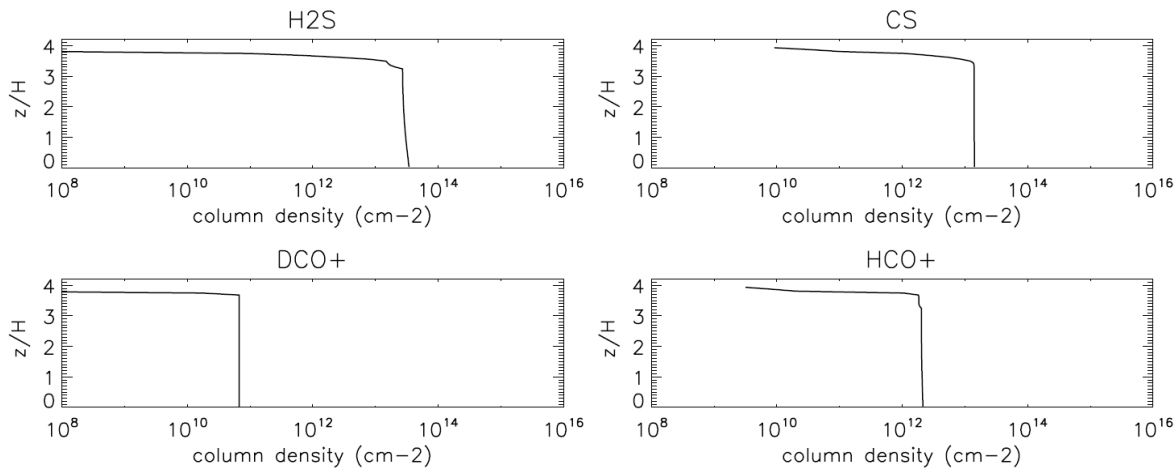


**Fig. 2.** Best model of H<sub>2</sub>S, CS, DCO<sup>+</sup>, and HCO<sup>+</sup> in the GG Tau A ring derived from Nautilus. The surface density is shown vs. the z/H ratio (z/H = 1 means 1 scale height).

**Table 2.** Observed and predicted surface densities (cm<sup>-2</sup>).

Detection			Non-detection		
Molecule	Observed <sup>a</sup> (derived from DiskFit)	Predicted <sup>c</sup> (from Nautilus)	Molecule	Observed <sup>a</sup> (derived from DiskFit)	Predicted <sup>c</sup> (from Nautilus)
HCO <sup>+</sup> (1–0)	$1.5 \pm 0.04 \times 10^{13}$	$2.2 \times 10^{12}$	CCS	$< 1.7 \times 10^{12}$	$7.2 \times 10^{10}$
H <sup>13</sup> CO <sup>+</sup> (2–1)	$5.3 \pm 0.3 \times 10^{11}$	(–)	SO <sub>2</sub>	$< 1.5 \times 10^{12}$	$6.0 \times 10^{12}$
DCO <sup>+</sup> (3–2)	$3.9 \pm 0.2 \times 10^{11}$	$7.0 \times 10^{10}$	SO	$< 1.1 \times 10^{12}$	$1.5 \times 10^{13}$
H <sub>2</sub> S 1(1,0)–1(0,1)	$1.3 \pm 0.1 \times 10^{12}$	$3.4 \times 10^{13}$	HC <sub>3</sub> N	$< 3.2 \times 10^{11}$	$5.7 \times 10^{11}$
CS(3–2)	$2.2 \times 10^{13b}$	$1.4 \times 10^{13}$	c-C <sub>3</sub> H <sub>2</sub>	$< 2.7 \times 10^{11}$	$2.4 \times 10^{12}$

**Notes.** <sup>(a)</sup>Observed surface density at 250 au is derived using DiskFit. <sup>(b)</sup>Phuong et al., in prep. <sup>(c)</sup>Species surface density in the gas phase at 250 au predicted with Nautilus. (–) Our model does not include carbon isotope chemistry.

- モデルを使って再現できないかやってみた
- DiskFit (輻射輸送)、Nautilus (gas, grain, grain mantleの3相gas-grain chemical model)
- H<sub>2</sub>Sの柱密度を合わせるとSO(non detection)ができすぎる。
- 化学進化計算のモデルがまだ不十分なのかも

## 36. Two Different Grain Size Distributions within the Protoplanetary Disk around HD 142527 Revealed by ALMA Polarization Observation

Satoshi Ohashi<sup>1</sup>, Akimasa Kataoka<sup>2</sup>, Hiroshi Nagai<sup>2</sup>, Munetake Momose<sup>3</sup>, Takayuki Muto<sup>4</sup>, Tomoyuki Hanawa<sup>5</sup>, Misato Fukagawa<sup>6</sup>, Takashi Tsukagoshi<sup>2,3</sup>, Kohji Murakawa<sup>7</sup> and Hiroshi Shibai<sup>8</sup>

- HD142527のpolarizationをALMAで観測した
- ダストのpolarized emissionには3つの理由が考えられる。
- 1. 磁場にalign、radiation gradientにalign、3. Self-scattering
- 北はself-scattering、南はgrain alignment by magnetic fields (self-scatteringは除外できない)
- 南はsmall dust grains ( $\lesssim 100$  microns)、北はmiddle-sized ( $\sim 100$  microns) grains と dominantなサイズが違うからでは
- 北のmiddle planeでは>cmのダストがあると考えられるが、optically thickで観測できなかった
- 南では磁場がtoroidal

# 36. つづき

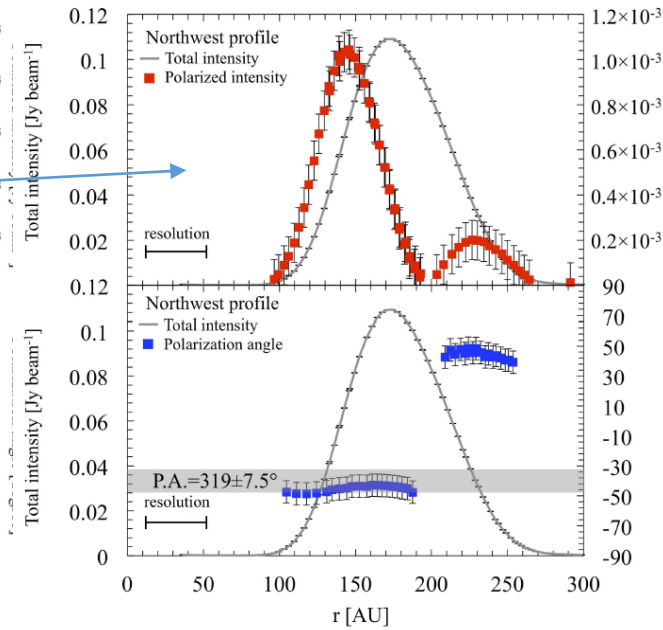
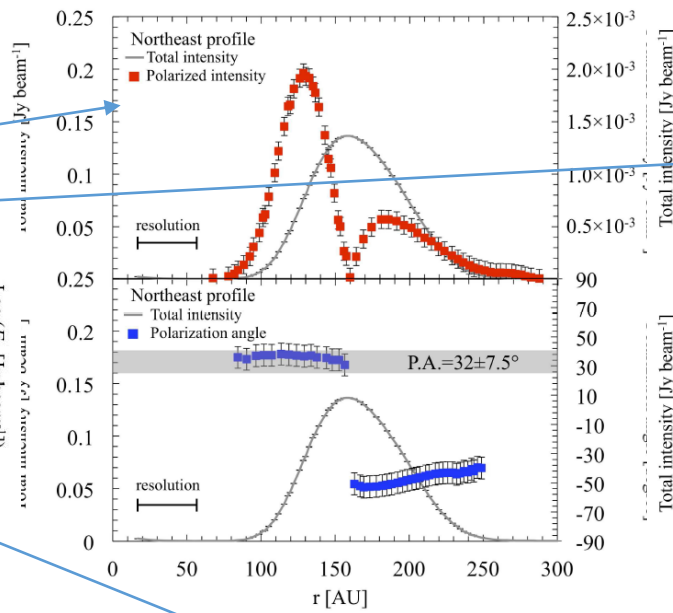
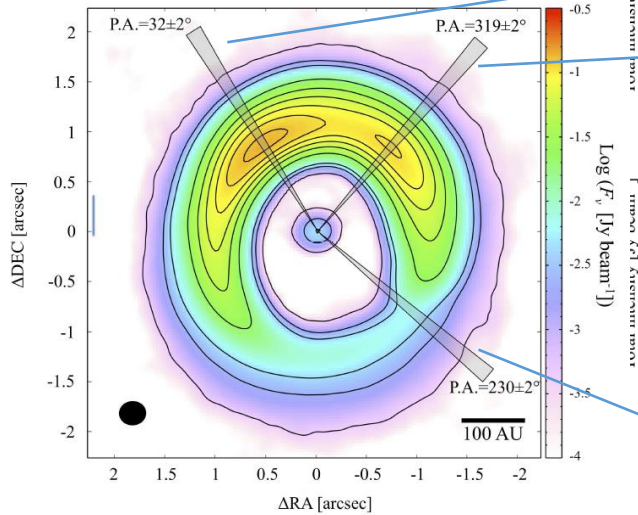


**Figure 3.** Upper panel: Radial profile of the total intensity (Stokes  $I$ , gray line) and the polarized intensity (red squares) at 0.87 mm for  $P.A. = 32 \pm 2^\circ$ . Lower panel: Radial profile of the total intensity (Stokes  $I$ , gray line) and the polarized intensity (red squares) at 0.87 mm for  $P.A. = 319 \pm 2^\circ$ . The polarization angle is shown in the bottom panel of the lower panel.

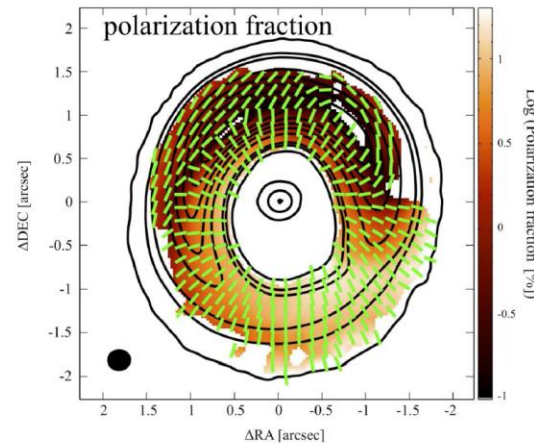
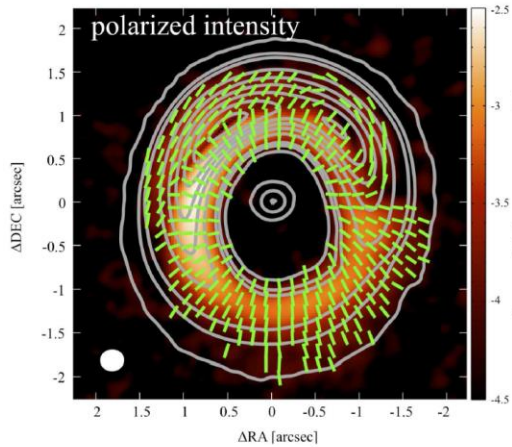
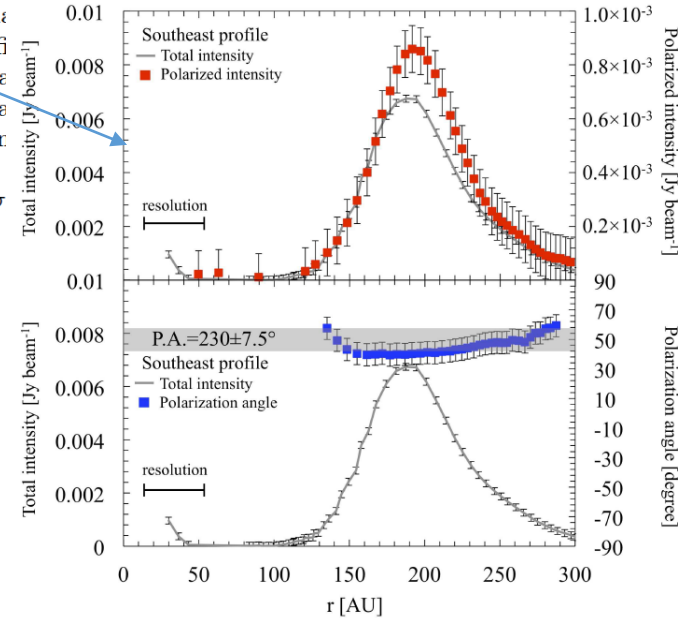


**Figure 2.** Polarized intensity and polarization fraction maps color-coded on a logarithmic scale. The contours show the continuum emission, and the green vectors are the polarization vectors. The polarization vectors and the polarization fraction are shown where the polarized intensity is higher than  $3\sigma_{PI}$ . Note that the lengths of the polarization vectors are set to be the



# 31. ALMA observations of the very young Class 0 protostellar system HH 211-mms: a 30-au dusty disk with a disk-wind traced by SO?

Chin-Fei Lee<sup>1,2</sup>, Zhi-Yun Li<sup>3</sup>, Naomi Hirano<sup>1</sup>, Hsien Shang<sup>1</sup>, Paul T.P. Ho<sup>1,4</sup>, and Qizhou Zhang<sup>5</sup>

HH 211-mms is one of the youngest Class 0 protostellar systems in Perseus at  $\sim 235$  pc away. We have mapped its central region at up to  $\sim 7$  AU ( $0''.03$ ) resolution. A dusty disk is seen deeply embedded in a flattened envelope, with an intensity jump in dust continuum at  $\sim 350$  GHz. It is nearly edge-on and is almost exactly perpendicular to the jet axis. It has a size of  $\sim 30$  au along the major axis. It is geometrically thick, indicating that the (sub)millimeter light emitting grains have yet to settle to the midplane. Its inner part is expected to have transformed into a Keplerian rotating disk with a radius of  $\sim 10$  au. A rotating disk atmosphere and a compact rotating bipolar outflow are detected in SO  $N_J = 8_9 - 7_8$ . The outflow fans out from the inner disk surfaces and is rotating in the same direction as the flattened envelope, and hence could trace a disk wind carrying away angular momentum from the inner disk. From the rotation of the disk atmosphere, the protostellar mass is estimated to be  $\lesssim 50 M_{\text{Jup}}$ . Together with results from the literature, our result favors a model where the disk radius grows linearly with the protostellar mass, as predicted by models of pre-stellar dense core evolution that asymptotes to an  $r^{-1}$  radial profile for both the column density and angular velocity.

## 32. New Young Stars and Brown Dwarfs in the Upper Scorpius Association

K.L. Luhman<sup>1,2</sup>, K.A. Herrmann<sup>3</sup>, E.E. Mamajek<sup>4,5</sup>, T.L. Esplin<sup>6</sup>, and M.J. Pecaut<sup>7</sup>

To improve the census of the Upper Sco association ( $\sim 11$  Myr,  $\sim 145$  pc), we have identified candidate members using parallaxes, proper motions, and color-magnitude diagrams from several wide-field imaging surveys and have obtained optical and infrared spectra of several hundred candidates to measure their spectral types and assess their membership. We also have performed spectroscopy on a smaller sample of previously known or suspected members to refine their spectral types and evidence of membership. We have classified 530 targets as members of Upper Sco, 377 of which lack previous spectroscopy. Our new compilation of all known members of the association contains 1631 objects. Although the census of Upper Sco has expanded significantly over the last decade, there remain hundreds of candidates that lack spectroscopy. The precise parallaxes and proper motions from the second data release of *Gaia* should extend down to substellar masses in Upper Sco, which will greatly facilitate the identification of the undiscovered members.

*Subject headings:* brown dwarfs — stars: formation — stars: low-mass — stars: luminosity function, mass function — stars: pre-main sequence

- Gaia DR1までしか使っていないので、DR2だともっとメンバーみつかるかも

# 33. Ejection processes in the young open cluster NGC 2264. A study of the [OI] $\lambda$ 6300 emission line - ERRATUM

P. McGinnis<sup>1,2</sup>, C. Dougados<sup>1</sup>, S. H. P. Alencar<sup>2,1</sup>, J. Bouvier<sup>1</sup> and S. Cabrit<sup>3</sup>

*Context.* Statistical studies of the spectral signatures of jets and winds in young stars are crucial to characterize outflows and understand their impact on disk and stellar evolution. The young, open cluster NGC 2264 contains hundreds of well-characterized classical T Tauri stars (CTTS), being thus an ideal site for these statistical studies. Its slightly older age than star forming regions studied in previous works, such as Taurus, allows us to investigate outflows in a different phase of CTTS evolution.

*Aims.* We search for correlations between the [OI] $\lambda$ 6300 line, a well-known tracer of jets and winds in young stars, and stellar, disk and accretion properties in NGC 2264, aiming to characterize the outflow phenomena that occur within the circumstellar environment of young stars.

*Methods.* We analyzed FLAMES spectra of 184 stars, detecting the [OI] $\lambda$ 6300 line in 108 CTTSs and two Herbig AeBe stars. We identified the main features of this line: a high-velocity component (HVC), and a broad and narrow low-velocity components (BLVC and NLVC). We calculated luminosities and kinematic properties of these components, then compared them with known stellar and accretion parameters.

*Results.* The luminosity of the [OI] $\lambda$ 6300 line and its components correlate positively with the stellar and accretion luminosity. The HVC is only detected among systems with optically thick inner disks; the BLVC is most common among thick disk systems and rarer among systems with anemic disks and transition disks; and the NLVC is detected among systems with all types of disks, including transition disks. Our BLVCs present blueshifts of up to  $50 \text{ km s}^{-1}$  and widths consistent with disk winds originating between  $\sim 0.05 \text{ au}$  and  $\sim 0.5 \text{ au}$  from the central object, while the NLVCs in our sample have widths compatible with an origin between  $\sim 0.5 \text{ au}$  and  $\sim 5 \text{ au}$ , in agreement with previous studies in Taurus.

A comparison of [OI] $\lambda$ 6300 profiles with CoRoT light curves shows that the HVC is found most often among sources with irregular, aperiodic photometric variability, usually associated with CTTSs accreting in an unstable regime. No stellar properties ( $T_{\text{eff}}$ , mass, rotation) appear to significantly influence any property of protostellar jets. We find jet velocities on average similar to those found in Taurus.

*Conclusions.* We confirm earlier findings in Taurus which favor an inner MHD disk wind as the origin of the BLVC, while there is no conclusive evidence that the NLVC traces photoevaporative disk winds. The [OI] $\lambda$ 6300 line profile shows signs of evolving as the disk disperses, with the HVC and BLVC disappearing as the inner disk becomes optically thin, in support of the scenario of inside-out gas dissipation in the inner disk.

**Key words.** accretion, accretion disks – line: formation – stars: jets – stars: pre-main sequence – stars: winds, outflows

# 34. Spectrally Resolved Mid-infrared Molecular Emission from Protoplanetary Disks and the Chemical Fingerprint of Planetesimal Formation

Joan R. Najita<sup>1</sup>, John S. Carr<sup>2</sup>, Colette Salyk<sup>3</sup>, John H. Lacy<sup>4</sup>, Matthew J. Richter<sup>5</sup> and Curtis DeWitt<sup>6</sup>

We present high-resolution spectroscopy of mid-infrared molecular emission from two very active T Tauri stars, AS 205 N and DR Tau. In addition to measuring high signal-to-noise line profiles of water, we report the first spectrally resolved mid-infrared line profiles of HCN emission from protoplanetary disks. The similar line profiles and temperatures of the HCN and water emission indicate that they arise in the same volume of the disk atmosphere, within 1–2 au of the star. The results support the earlier suggestion that the observed trend of increasing HCN/water emission with disk mass is a chemical fingerprint of planetesimal formation and core accretion in action. In addition to directly constraining the emitting radii of the molecules, the high-resolution spectra also help break degeneracies between temperature and column density in deriving molecular abundances from low-resolution mid-infrared spectra. As a result, they can improve our understanding of the extent to which inner disks are chemically active. Contrary to predictions from HCN excitation studies carried out for AS 205 N, the mid-infrared and near-infrared line profiles of HCN are remarkably similar. The discrepancy may indicate that HCN is not abundant beyond a few au or that infrared pumping of HCN does not dominate at these distances.

*Key words:* circumstellar matter – planets and satellites: formation – protoplanetary disks – stars: pre-main sequence

# 35. The Surface Magnetic Activity of the Weak-Line T Tauri Stars TWA 9A and V1095 Sco

B. A. Nicholson,<sup>1,2</sup> G. A. J. Hussain,<sup>2,3,4</sup> J.-F. Donati,<sup>3,4</sup> C. P. Folsom,<sup>3,4</sup> M. Mengel,<sup>1</sup> B. D. Carter,<sup>1</sup> D. Wright,<sup>1</sup> and the MaTYSSE collaboration

## ABSTRACT

We present a detailed analysis of high-resolution spectropolarimetric observations of the weak-line T Tauri stars (wTTs) TWA 9A and V1095 Sco as part of a wider survey of magnetic properties and activity in weak-line T Tauri stars, called MaTYSSE (Magnetic Topologies of Young Stars and the Survival of close-in giant Exoplanets). Our targets have similar masses but differing ages which span the stage of radiative core formation in solar-mass stars. We use the intensity line profiles to reconstruct surface brightness maps for both stars. The reconstructed brightness maps for TWA 9A and V1095 Sco were used to model and subtract the activity-induced jitter, reducing the RMS in the radial velocity measurements of TWA 9A by a factor of  $\sim 7$ , and for V1095 Sco by a factor of  $\sim 3$ . We detect significant circular polarisation for both stars, but only acquired a high quality circular polarisation time-series for TWA 9A. Our reconstructed large-scale magnetic field distribution of TWA 9A indicates a strong, non-axisymmetric field. We also analyse the chromospheric activity of both stars by investigating their H $\alpha$  emission, finding excess blue-ward emission for most observations of V1095 Sco, and symmetric, double-peaked emission for TWA 9A, with enhanced emission at one epoch likely indicating a flaring event.

**Key words:** stars: magnetic fields, techniques: polarimetric, stars: formation, stars: imaging, stars: individual: TWA 9A, stars: individual: V1095 Sco.

# 38. Mapping the $^{13}\text{CO}/\text{C}^{18}\text{O}$ abundance ratio in the massive star forming region G29.96–0.02

S. Paron<sup>1,2</sup>, M.B. Areal<sup>1</sup>, and M.E. Ortega<sup>1</sup>

**Aims.** Estimating molecular abundances ratios from the direct measurement of the emission of the molecules towards a variety of interstellar environments is indeed very useful to advance in our understanding of the chemical evolution of the Galaxy, and hence of the physical processes related to the chemistry. It is necessary to increase the sample of molecular clouds, located at different distances, in which the behaviour of molecular abundance ratios, such as the  $^{13}\text{CO}/\text{C}^{18}\text{O}$  ratio, is studied in detail.

**Methods.** We selected the well-studied high-mass star-forming region G29.96–0.02, located at a distance of about 6.2 kpc, which is an ideal laboratory to perform this kind of studies. To study the  $^{13}\text{CO}/\text{C}^{18}\text{O}$  abundance ratio ( $X^{13/18}$ ) towards this region it was used  $^{12}\text{CO}$  J=3–2 data obtained from the CO High-Resolution Survey,  $^{13}\text{CO}$  and  $\text{C}^{18}\text{O}$  J=3–2 data from the  $^{13}\text{CO}/\text{C}^{18}\text{O}$  (J=3–2) Heterodyne Inner Milky Way Plane Survey, and  $^{13}\text{CO}$  and  $\text{C}^{18}\text{O}$  J=2–1 data retrieved from the CDS database which were observed with the IRAM 30 m telescope. The distribution of column densities and  $X^{13/18}$  throughout the extension of the analyzed molecular cloud was studied based on LTE and non-LTE methods.

**Results.** Values of  $X^{13/18}$  between 1.5 to 10.5, with an average of about 5, were found across the studied region, showing that, besides the dependency between  $X^{13/18}$  and the galactocentric distance, the local physical conditions may strongly affect this abundance ratio. We found that correlating the  $X^{13/18}$  map with the location of the ionized gas and dark clouds allows us to suggest in which regions the far-UV radiation stalls in dense gaseous components, and in which ones it escapes and selectively photodissociates the  $\text{C}^{18}\text{O}$  isotope. The non-LTE analysis shows that the molecular gas has very different physical conditions, not only spatially across the cloud, but also along the line of sight. This kind of studies may represent a tool to indirectly estimate (from molecular lines observations) the degree of photodissociation in molecular clouds, which is indeed useful to study the chemistry in the interstellar medium.

**Key words.** ISM: abundances – ISM: molecules – Galaxy: abundances – (*ISM:*) HII regions – Stars: formation